Electronic Supplementary Material (ESI) for Lab on a Chip.


# Supplementary Information

# Microfluidic cryofixation for correlative microscopy

**Y. X. Mejia[1], H. Feindt[2], D. Zhang[1], S. Steltenkamp[2], T.P. Burg[1]***

[1] *Max Planck Institute for Biophysical Chemistry, Am Fassberg 11, 37077 Goettingen, Germany*
[2] *Micro Systems Technology (MST), Center of Advanced European Studies and Research (caesar), Ludwig-Erhard-Allee 2, 53175 Bonn, Germany*

*corresponding author

## 1. Background

Due to their ability to control small volumes, microfluidic devices are ideal for use in applications where localized heating and cooling with fast time scales is required. For this reason, microfluidic systems have been used previously for studies of ice formation[1-4], for creating valves by exploiting local temperature-induced phase changes[5-7] and for cryogenic cooling of magnetic resonance coils[8]. For microscopy applications, Chung et al.[9] demonstrated a clever scheme based on cooling a portion of a microfluidic channel to 4 °C in order to temporarily immobilize and image small nematodes. Microfluidic methods have also been applied to the study of the effects of different cryoprotectants on cell morphology and viability[10, 11], as well as for the fast mixing of solutions that are quickly frozen once they exit the device[12, 13].

Microfluidic platforms have also proven to be advantageous for the manipulation and imaging of a wide variety of cell culture systems. In fact, the growth and viability of a wide range of cell types and small organisms within microfluidic channels has already been demonstrated[14-16]. However, factors like surface treatment, shear stress and adequate nutrient supply have to be considered.

## 2. Device fabrication, assembly, and operation

Micromachined components of the microfluidic cryofixation device: The novel fabrication procedure used in the construction of our microfluidic cryofixation device has been designed so as to maximize freezing rates. The microfluidic cryofixation device consists of three key components, as shown in Fig. S1a. First, a silicon wafer was patterned using SU8-5 and silanized to serve as a master for the fabrication of the PDMS microchannel. PDMS is a flexible polymer that retains excellent mechanical stability and optical clarity at cryogenic temperatures. Second, a silicon chip, termed the 'fluidic chip', was made by dry etching of single crystal silicon. The fluidic chip is used to deliver fluid to the thin PDMS channel, which would otherwise be inaccessible due to its small dimensions. This chip contains patterned bypass channels on the top (Fig. S1a, top view, white lines) and connecting through-holes to the bottom (Fig. S1a, bottom view). It also contains a 1 mm circular opening in the center. The through-silicon fluidic vias and bypass channels of the fluidic chip were made in a two-step deep reactive ion etching (DRIE) process using a combination of photoresist and $SiO_2$ as masks. In this process, the wafers were first thermally oxidized (~1 µm) and the bypass channels were defined by etching the oxide layer in buffered oxide etch (BOE). Next, photoresist was spun and patterned with a mask that revealed the through-holes. These holes were subsequently etched to a depth of 50-100 µm less than the thickness of the silicon. The photoresist mask was then stripped, and etching was continued to finish the through-holes and, at the same time, etch the bypass channels, which were masked by the patterned $SiO_2$. The third component in the system is the heater chip. The micro-heater was fabricated by sputtering a 900 nm layer of nickel-chrome (NiCr, 80/20) followed by a 350 nm layer of aluminum on a double side polished wafer with a 2.5 µm thermal oxide layer as a thermal and electrical insulator. The layers were wet etched so as to form a thin 200 µm wide strip of NiCr connected to a printed circuit board via wire bonded aluminum traces (see also. Fig. S2d).

Assembly of the microfabricated components: The three micromachined components that make up the microfluidic cryofixation device are assembled as shown schematically in Fig. S1b. First, a thin

PDMS layer is spin coated on a fluorosilane-coated silicon master. A thin layer of parylene is then deposited to give the PDMS layer enough rigidity to be peeled off the master (Fig. S1b, 1-3). A second PDMS layer is then spin coated on a blank fluorosilane-treated wafer and cured at 80 °C. Next, two holes are lasercut in the PDMS and the layer is plasma-bonded to the bottom side of the fluidic chip. The membrane with the patterend channel is then bonded to the fluidic chip so as to form a closed microchannel with an inlet and an outlet to the bypass channels (Fig. S1b, 4-6). A third layer of PDMS is used to close the bypass channels on the top side of the fluidic chip (Fig. S1b, 7). Last, the finished micro-fluidic device is aligned to the heater chip using a micromanipulator so that the channel fits entirely inside the heater area. The alignment between the two chips is then fixed by a UV-cured adhesive.

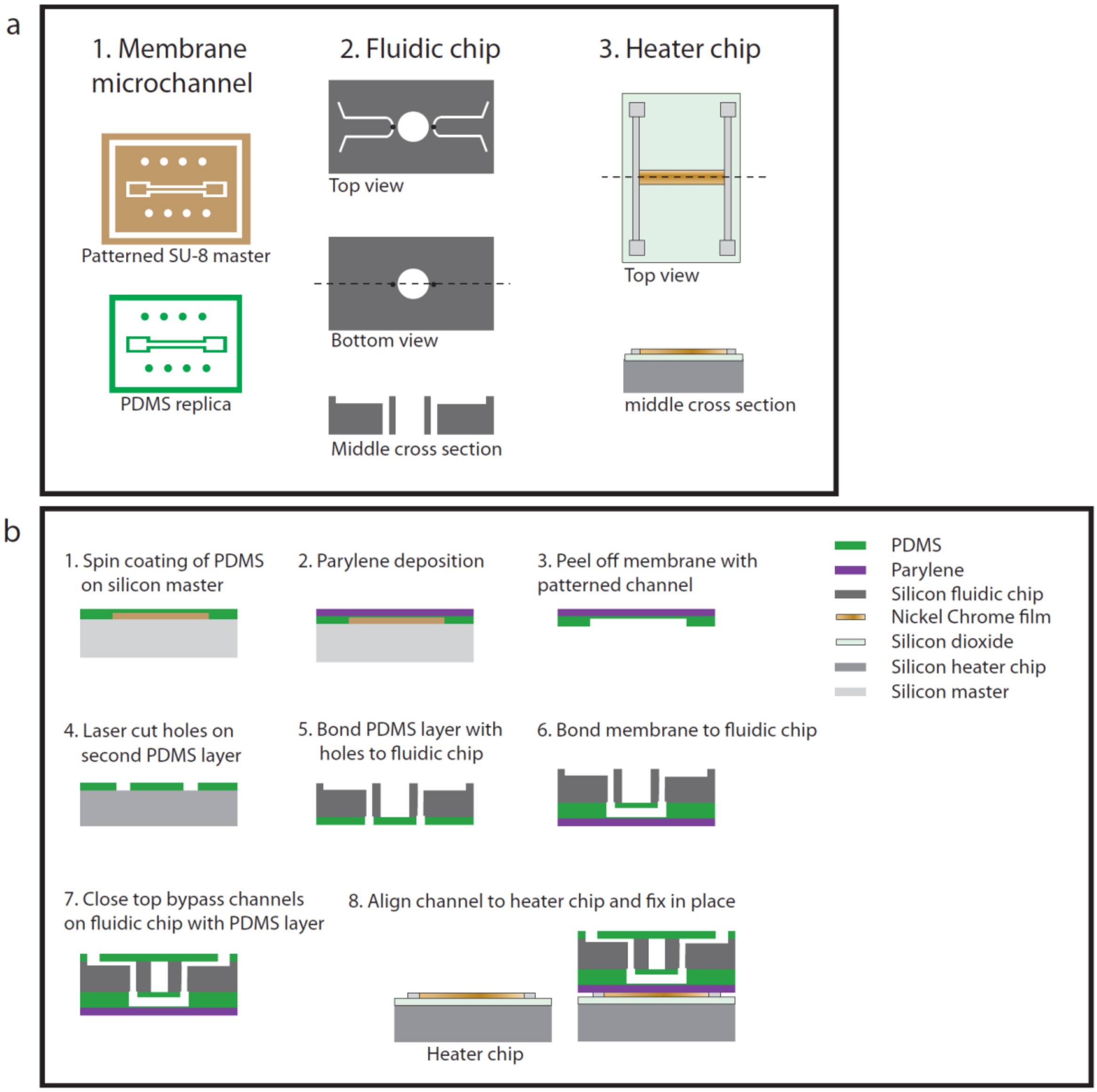


**Figure S1:** (a) Layout of main components in the microfluidic cryofixation device: 1. PDMS foil with embedded fluidic channel made by soft lithography, 2. Fluidic chip made of silicon, 3. Thin-film resistive heater chip. (b) Assembly of the components.

<u>Assembly of the system:</u> Fig. S2 explains the assembly of the complete system. The key to obtaining high cooling rates and thereby suppressing ice crystallization is the low thermal mass of the fluidic device. The microchannel is therefore embedded inside a PDMS foil only ~40 µm thick, which spans a

1 mm circular opening in the fluidic chip. To further reduce thermal mass the channel is formed by 50 µm thick walls flanked on the outside by an insulating air space (Fig. S2a-c, and Fig. S2f). The electrical heater is a 200 µm wide NiCr strip connecting two aluminum traces in an H-configuration (Fig. S2d). The fluidic chip and the heater chip are aligned such that their long axes are perpendicular to each other and the fluidic channel is parallel and on top of the heater such that the channel fits entirely inside the heated strip. (Fig. S2e). The alignment is done as follows: First, the heater chip is glued to two glass supports, shown at the top and bottom of Fig. S2e. It is then loosely placed into the copper frame. The fluidic chip is then put on top and mechanically clamped to the frame. Next, the heater chip is aligned to the channel in X, Y, and Theta (in the plane of Fig. S2e) using a micromanipulator. Finally, the two chips are brought into hard contact with the channel sandwiched between them. At this point, a small amount of UV-adhesive is cured between the glass pieces and the copper frame. This fixes the alignment. Since the copper frame remains warm throughout the experiment, the adhesive joint is not subjected to large temperature variations. Samples are injected into bypasses on the fluidic chip through two PDMS manifolds (shown in clear green in Fig. S2e). A close up of the flow path and of the alignment between the suspended microchannel and the heater strip is shown in Fig. S2f. Note how the silicon chip distributes fluid to the PDMS microchannel and keeps the incoming liquid warm despite being in close proximity to a cold surface underneath.

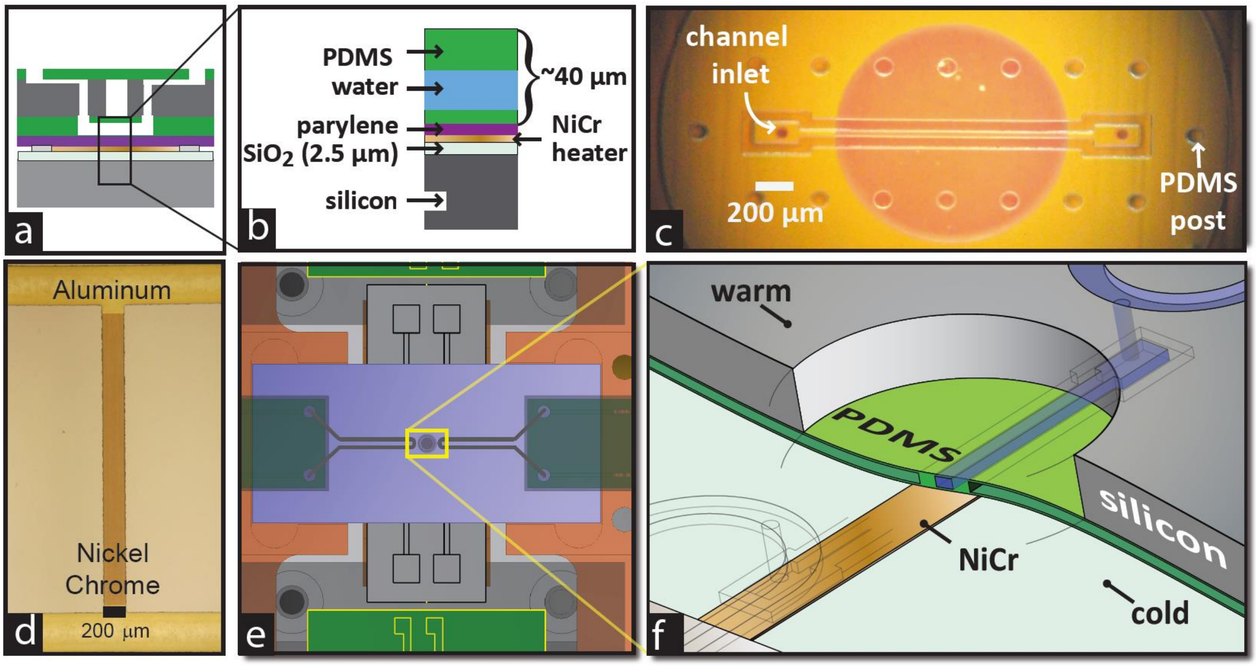


**Figure S2:** Detailed assembly of the microfluidic cryofixation system. (a) Cross-section diagram of the fluidic chip with bonded PDMS microchannel aligned with the heater chip, fabricated according to Fig. S1b. (b) Magnified section of the fluidic layers in the suspended region of the channel. (c) Optical micrograph of the channel, channel inlets, and the 1 mm circular opening in the fluidic chip through which optical observation is done. (d) Optical micrograph of the thin-film micro-heater. (e) Top view schematic of the relative arrangement of the fluidic chip (blue) and the heater chip (grey) after alignment. (f) Section view of the aligned fluidic chip and heater chip showing the suspended channel embedded in the thin PDMS foil that spans the 1 mm hole in the fluidic chip.

Device operation: The assembly is placed on top of the cryogenic stage such that only the heater chip is in direct contact with the cold surface. The heater chip serves as a combined heat sink (silicon), thermal insulator over which the thermal gradient drops ($SiO_2$), and mechanical connection point. During the experiment, the heater chip is kept cold by means of a cryogenic stage cooled by a constant flow of liquid nitrogen. Approximately 30 – 40 W of power is supplied to the heater during operation to keep the contents of the microchannel at room temperature. This power is adjusted using the resistivity of the thin-film heater itself as a measure of temperature. Fig. S3 illustrates the temperature zones in the system as the channel is cycled between room temperature and low temperature. The copper frame and the fluidic chip remain at room temperature throughout the experiment. While the heater is on, there is a steep temperature gradient across the thermal oxide layer of the heater chip. Minor gradients also build up in the warm parts, but due to the high thermal conductivity of silicon and copper, these are sufficiently small to allow the continuous flow of fluid through the different layers into and out of the PDMS channel. When the power is shut off, the thin PDMS foil on top of the heater is the only part that experiences a strong drop in temperature. After freezing, there is a temperature gradient in the inlet and outlet of the PDMS channel. Cooling is less rapid in this transition zone, and ice formation is therefore expected. However, it is important to note that this does not affect the central part of the PDMS channel seen in the microscope, where heat is dissipated vertically with great efficiency into the liquid nitrogen cooled sink.

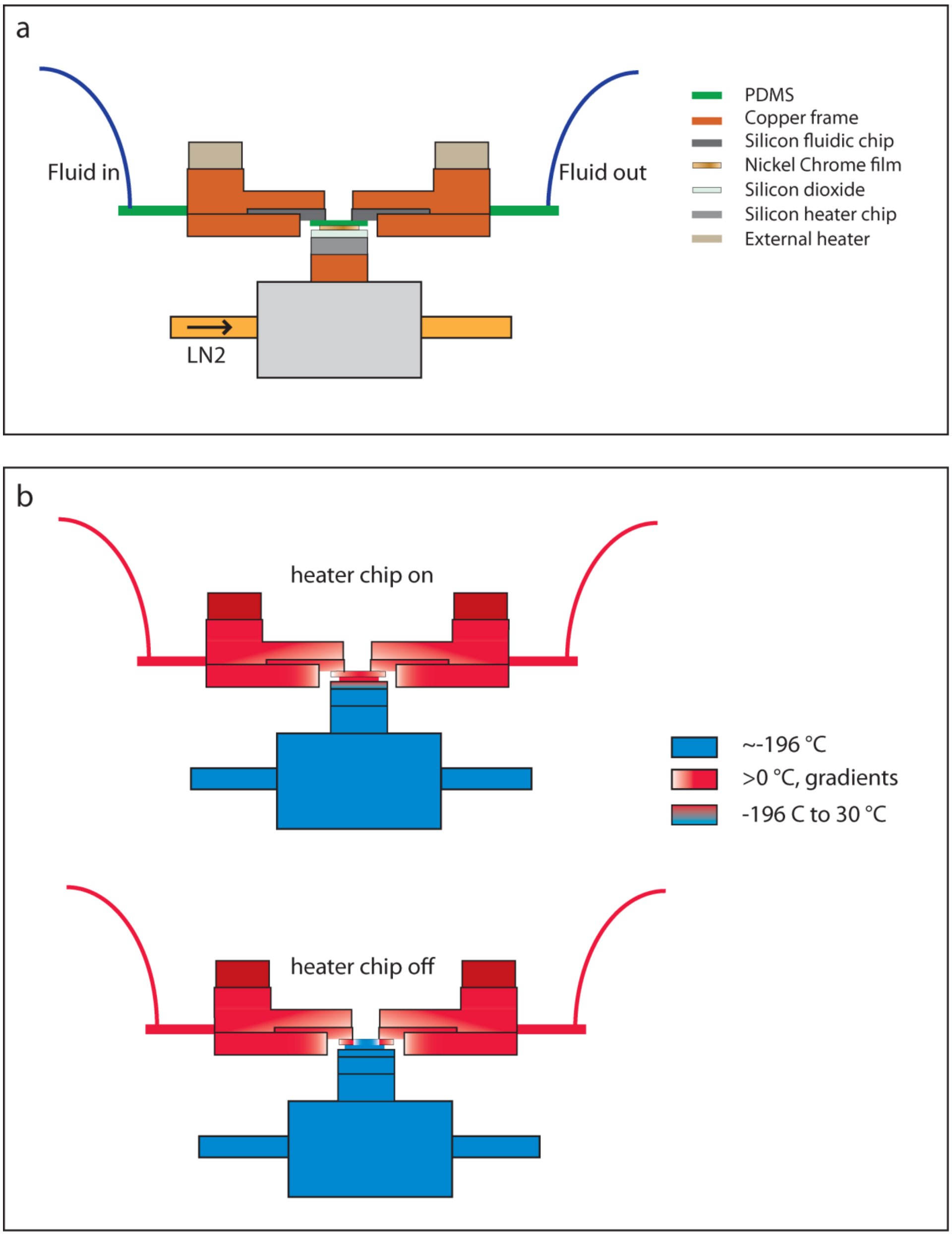


**Figure S3:** Schematic of heat transfer and temperature gradients of the microfluidic cryofixation device. a) Side section of the device shown in Fig. 2. b) Schematic of the temperature gradients present when the heater is on and off. When the micro heater is on, the silicon dioxide insulator on the heater chip maintains a very steep temperature gradient: from liquid nitrogen temperature to temperatures above 0 °C. The heat provided by the heater chip keeps the solution inside the PDMS channel liquid. In addition, for fluid flow to be possible, the complete path from the fluid inlet to the outlet must be kept above 0°C. This is ensured by external heaters providing heat to the copper frame, which in turn keeps the fluidic silicon chip at temperatures above freezing. When the micro-heater is off, fluid flow is interrupted by the frozen channel.

## 3. Cell culture and viability of yeast cells in YPD + 800 mM sorbitol

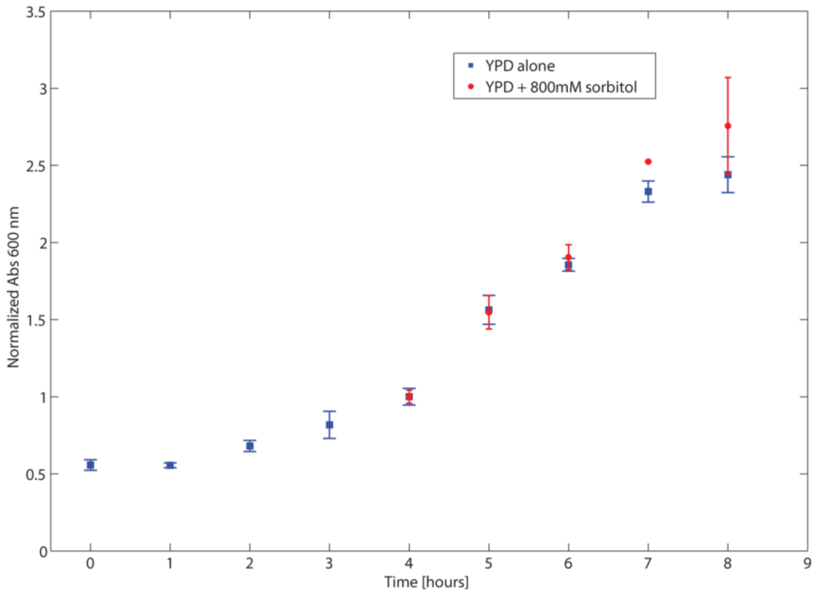


**Figure S4:** Comparison of growth curves for yeast cells in YPD alone and YPD supplemented with 800 mM sorbitol as a cryoprotectant.

To ensure that yeast growth is not hindered by the addition of sorbitol, we compared growth curves with and without the additive. An overnight yeast culture was diluted in fresh YPD and incubated at 30 °C. Growth was measured every hour using a Nanodrop 2000c and measuring absorbance at 600 nm. After three hours of incubation, half of the culture was spun down and resuspended in YPD+800 mM of sorbitol. Both cultures were incubated at 30 °C for a total of 8 hours. Measurements were normalized by the value at t = 4 h. The presence of 800 mM sorbitol does not cause any significant reduction in growth rate.

Yeast cells for all freezing experiments were grown in YPD at 30 °C and re-suspended in PM (0.5% peptone, 0.17% YNB, 2% glucose, 40 μg/mL uracil) with 800 mM sorbitol as a cryoprotectant. PM is a media with low autofluorescence.

## 4. Freezing and thawing dynamics

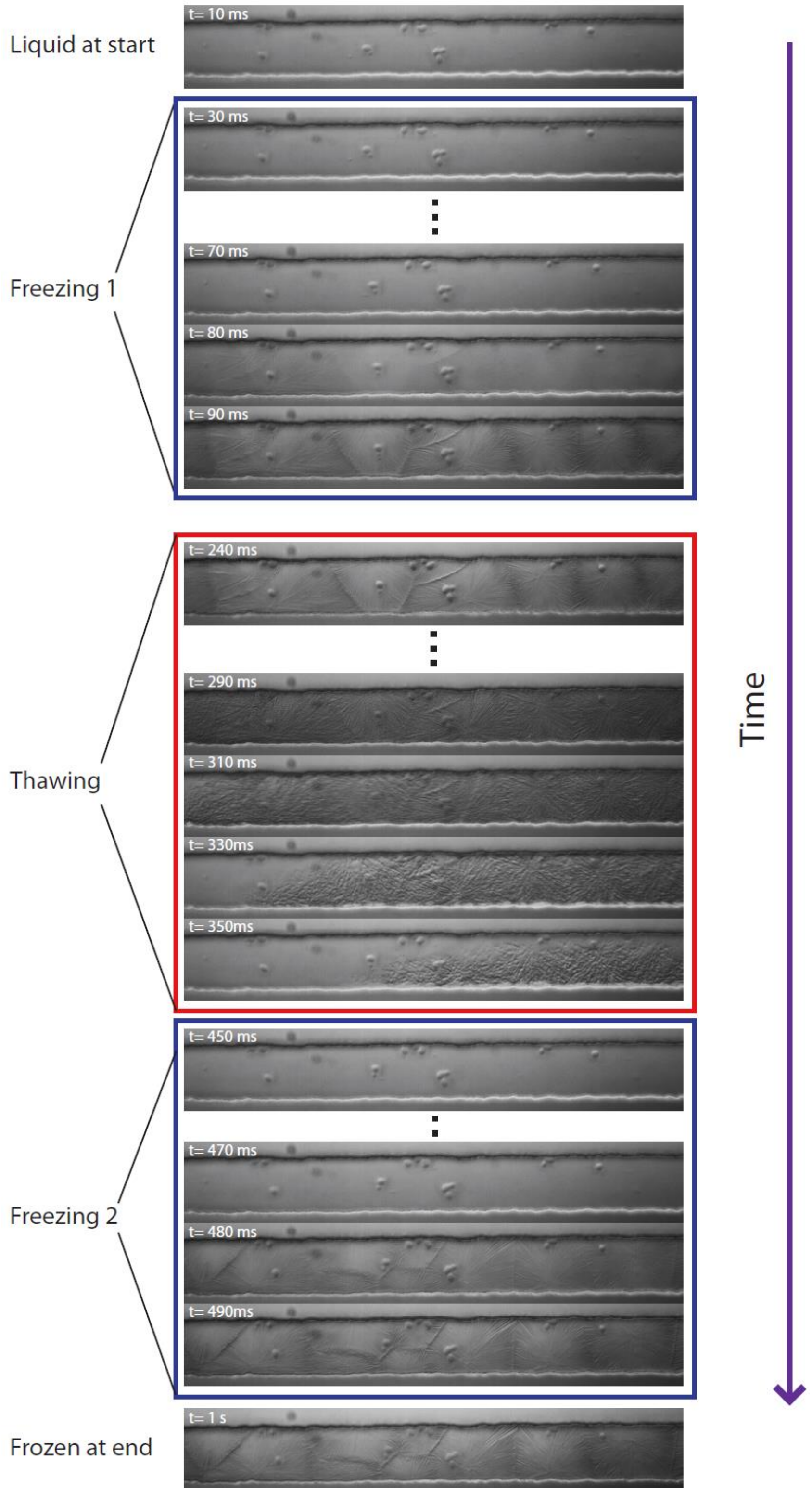


**Figure S5:**

Two consecutive freezing cycles with intermediate thawing are visualized here by the formation and dissolution of crystalline ice in YPD + 10% (v/v) ethanol. At time t = 10 ms the heater chip is on so that the solution in the channel is liquid. The heater is then turned off (Freezing 1) so that the solution solidifies. The system allows real-time observation of the dynamics of ice formation. The heater is then turned on (Thawing) and the ice crystals start to slowly disappear. The heater is turned off again (Freezing 2) and ice crystals quickly re-form. Images were taken with a 40x air objective and a 10 ms exposure time.

One possible application of the current system is the study of ice formation and thawing in microfluidic channels at heating and cooling rates on the order of $10^4$ °C/s. An example of such an experiment is shown in Fig. S5. A solution of YPD containing 10% (v/v) ethanol as cryoprotectant is cycled between room temperature and the base temperature of the liquid nitrogen cooled stage by turning on and off the heater. Differential interference contrast (DIC) imaging reveals the formation of crystalline ice, as this mode is highly sensitive to gradients in refractive index. The experiment shown in Fig. S5 allows an approximate estimate of the heating and cooling rates achieved by the system based on the thawing process. As can be seen in the middle panel (red box), the morphology of the ice changes visibly within the first 30 ms, and visible melting sets in between 50 and 70 ms after activating the heater. Based on a simple exponential approximation to the cooling and heating curve, and considering a freezing point of approximately -5°C for this ethanol/water mixture, the time constant can be obtained. The result confirms that the mean rate over the first 50 °C of the temperature jump is on the order of 7,500 – 10,000 °C/s. Although the geometry and fabrication process have not been optimized, these results reveal heating and cooling rates two orders of magnitude faster than previously reported for microfluidic systems[1] .

## 5. Incorporation into a correlative microscopy workflow

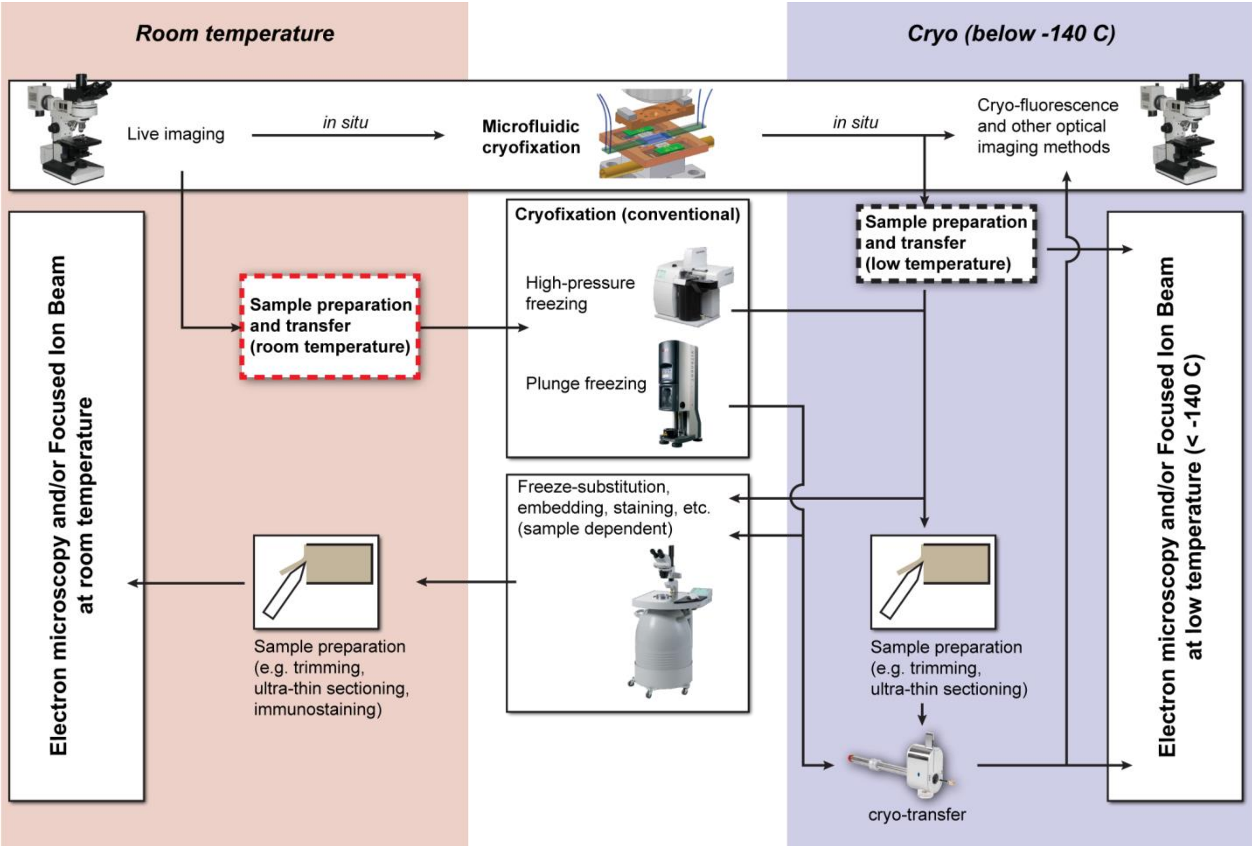


**Figure S6:** Microfluidic cryofixation in relation to high-pressure freezing and plunge freezing based workflows for correlative light and electron microscopy. The key benefit of the microfluidic approach described here is to eliminate all transfer and sample preparation steps between live imaging and cryofixation (red box). An additional cryo-transfer step can in principle interface the microfluidic device to existing sectioning, cryo-FIB, and freeze substitution technologies (black dashed outline); this interface is currently being developed.

## 6. Perspectives on optical cryo-imaging of frozen samples

Our microfluidic cryofixation method enables the optical imaging of frozen samples immediately after freezing and without the need for transfer protocols or tools. Hence this method eliminates the risk of de-vitrification or ice contamination of the sample. Furthermore, one additional benefit of cryofixation inside microfluidic channels is that objects that are normally in suspension, such as non-adherent cells, can be imaged free from motion-induced blur. This is of particular interest in 3D confocal microscopy, where long acquisition periods can be required to assemble a full Z-stack. Other well-known advantages of cryo-optical imaging include narrow line widths, large cross sections, and dramatically improved photostability [17-19]. In fact, recently there has been significant interest in the development and use of cryogenic stages for fluorescence cryo-microscopy for correlative imaging with electron cryo-microscopy [20-22] and for superresolution fluorescence microscopy [23, 24].

A universal limitation in optical imaging at low temperature is that no cryo-immersion objectives are commercially available for the inspection of the frozen sample with high numerical aperture. Our current system uses a Zeiss LD Plan-Neofluar 40x/0.6 NA air objective . Modifications to the top cover of the copper holder would allow the use of other air objectives with a shorter working distance and higher numerical aperture (e.g. Zeiss LD Plan-Neofluar 63x/0.75, Mitutoyo Plan Apo HR 100x/0.9). Numerical apertures higher than 1, and the consequent increase in spatial resolution, are only possible using immersion objectives. Unfortunately, the identification, characterization and use of appropriate immersion fluids that remain liquid at temperatures -140C or lower, and that minimize aberrations due to index of refraction mismatch or thermal gradient effects still remains a challenge. Nonetheless, some progress in developing such objectives has been made in recent years[25, 26].

1. C. A. Stan, G. F. Schneider, S. S. Shevkoplyas, M. Hashimoto, M. Ibanescu, B. J. Wiley and G. M. Whitesides, *Lab on a chip*, 2009, **9**, 2293-2305.
2. J. F. Edd, K. J. Humphry, D. Irimia, D. A. Weitz and M. Toner, *Lab on a chip*, 2009, **9**, 1859-1865.
3. S. Park, P. A. L. Wijethunga, H. Moon and B. Han, *Lab on a chip*, 2011, **11**, 2212-2221.
4. Y. Celik, R. Drori, N. Pertaya-Braun, A. Altan, T. Barton, M. Bar-Dolev, A. Groisman, P. L. Davies and I. Braslavsky, *Proceedings of the National Academy of Sciences of the United States of America*, 2013, **110**, 1309-1314.
5. Z. Y. Chen, J. Wang, S. Z. Qian and H. H. Bau, *Lab on a chip*, 2005, **5**, 1277-1285.
6. A. E. Sgro, P. B. Allen and D. T. Chiu, *Anal Chem*, 2007, **79**, 4845-4851.
7. L. Gui, B. Y. Yu, C. L. Ren and J. P. Huissoon, *Microfluidics and nanofluidics*, 2011, **10**, 435-445.
8. C. Koo, R. F. Godley, J. Park, M. P. McDougall, S. M. Wright and A. Han, *Lab on a chip*, 2011, **11**, 2197-2203.
9. K. Chung, M. M. Crane and H. Lu, *Nature methods*, 2008, **5**, 637-643.
10. Y. S. Song, S. Moon, L. Hulli, S. K. Hasan, E. Kayaalp and U. Demirci, *Lab on a chip*, 2009, **9**, 1874-1881.
11. Y. S. Heo, H. J. Lee, B. A. Hassell, D. Irimia, T. L. Toth, H. Elmoazzen and M. Toner, *Lab on a chip*, 2011, **11**, 3530-3537.
12. Y. Lin, G. J. Gerfen, D. L. Rousseau and S. R. Yeh, *Analytical Chemistry*, 2003, **75**, 5381-5386.
13. J. Lee, A. K. Jha, A. Bose and A. Tripathi, *Langmuir : the ACS journal of surfaces and colloids*, 2008, **24**, 12738-12741.
14. A. Ben-Yakar, N. Chronis and H. Lu, *Curr Opin Neurobiol*, 2009, **19**, 561-567.
15. I. Meyvantsson and D. J. Beebe, *Annu Rev Anal Chem*, 2008, **1**, 423-449.
16. C. E. Sims and N. L. Allbritton, *Lab on a chip*, 2007, **7**, 423-440.
17. C. L. Schwartz, V. I. Sarbash, F. I. Ataullakhanov, J. R. Mcintosh and D. Nicastro, *Journal of microscopy*, 2007, **227**, 98-109.
18. K. Mauring, J. Deich, F. I. Rosell, T. B. McAnaney, W. E. Moerner and S. G. Boxer, *The journal of physical chemistry. B*, 2005, **109**, 12976-12981.
19. E. Betzig, G. H. Patterson, R. Sougrat, O. W. Lindwasser, S. Olenych, J. S. Bonifacino, M. W. Davidson, J. Lippincott-Schwartz and H. F. Hess, *Science*, 2006, **313**, 1642-1645.
20. A. Sartori, R. Gatz, F. Beck, A. Rigort, W. Baumeister and J. M. Plitzko, *Journal of structural biology*, 2007, **160**, 135-145.
21. L. F. van Driel, J. A. Valentijn, K. M. Valentijn, R. I. Koning and A. J. Koster, *European journal of cell biology*, 2009, **88**, 669-684.
22. A. Rigort, F. J. Bauerlein, A. Leis, M. Gruska, C. Hoffmann, T. Laugks, U. Bohm, M. Eibauer, H. Gnaegi, W. Baumeister and J. M. Plitzko, *Journal of structural biology*, 2010, **172**, 169-179.
23. R. Kaufmann, P. Schellenberger, E. Seiradake, I. M. Dobbie, E. Y. Jones, I. Davis, C. Hagen and K. Grunewald, *Nano letters*, 2014.
24. Y. W. Chang, S. Chen, E. I. Tocheva, A. Treuner-Lange, S. Lobach, L. Sogaard-Andersen and G. J. Jensen, *Nature methods*, 2014.
25. M. A. Le Gros, G. McDermott, M. Uchida, C. G. Knoechel and C. A. Larabell, *Journal of microscopy*, 2009, **235**, 1-8.
26. E. A. Smith, B. P. Cinquin, M. Do, G. McDermott, M. A. Le Gros and C. A. Larabell, *Ultramicroscopy*, 2013.